

Effects of Electromagnetic Coupling on Conductance Switching of a Gated Tunnel Junction

Adva Baratz,[†] Alexander J. White,^{‡,||} Michael Galperin,[‡] and Roi Baer^{*,§}

[†]Department of Environmental Physics, Israel Institute for Biological Research, P.O.B. 19, Ness-Ziona 74100, Israel

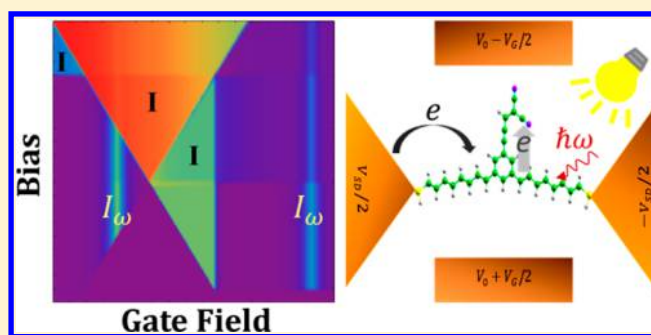
[‡]Department of Chemistry and Biochemistry, University of California at San Diego, La Jolla, California 92093, United States

^{||}Theoretical Division, Center for Nonlinear Studies (CNLS), Los Alamos National Laboratory, Los Alamos, New Mexico 87545, United States

[§]Fritz Haber Center for Molecular Dynamics, Institute of Chemistry, The Hebrew University of Jerusalem, Jerusalem 91904, Israel

ABSTRACT: Using a combination of density functional theory and quantum master equations approach, we study the effect of electromagnetic (EM) coupling on the non-equilibrium steady-state behavior of a recently introduced gated molecular junction. This junction was demonstrated in a previous publication to exhibit sharp current switching near a certain critical DC field E_z^* , which induces intramolecular charge transfer, and here, we analyze the steady-state population and current when an AC EM field (EMF) is present. The AC EMF at frequency ω_0 produces pronounced population and current features at gate fields $E_z = E_z^* \pm \hbar\omega_0/ez$ (where ez is the dipole of the charge-transfer state) and thus allows additional sharp switching capability at lower gate fields. We found that even when EMF is absent, the EM coupling itself changes the overall steady-state population and current distributions because it allows for relaxation via spontaneous emission.

SECTION: Energy Conversion and Storage; Energy and Charge Transport



Using light to switch the conductance of a molecular junction is a long-standing challenge.^{1–8} The mechanism of switching is often based on the change of nuclear conformation following absorption of light. However, “non-mechanical” switching mechanisms have also been suggested, involving exciton–plasmon interactions and heating,^{9,10} and electron transfer combined with a Coulomb blockade effect.^{11,12} In the latter work by the present authors, the molecular junction was weakly coupled to source and drain (SD) electrodes, and a gate acted as an on/off switch for the intrajunction electron transfer between localized donor and acceptor sites separated by a distance z . A schematic depiction of the system is given in Figure 1. The gate field E_z in this setup has several roles. It changes the energy difference between the ground state (GS) and the charge-transfer (CT) excited state. The second role is that of a switch; beyond a critical value $E_z > E_z^* = (I - A)/ez$, where I and A are the ionization and electron affinity, respectively, and e is the electron charge, the CT occurs spontaneously, and the CT state becomes the GS. One can also view this from the perspective of conductance through quasiparticle (QP) levels; for $E_z > E_z^*$, the highest occupied level, ψ_H , located on the donor group, is doubly occupied, while the lowest unoccupied level, ψ_L , located on the acceptor group is empty. In this regime, conductance readily goes through ψ_L , while it is blocked in ψ_H by destructive interference. The gap E_g between these QP levels can be reduced by increasing E_z , and at the critical gate, when $E_z = E_z^*$, an electron transfers

spontaneously from ψ_H to ψ_L , causing an energetic rearrangement. ψ_L obtains an electron of, say, spin up from the donor and becomes a hole-current conductor, while the energy of the down spin component gets Coulomb-blocked (shoots up in energy). A description of the junction taking electron correlation into account, using a Hubbard model, reveals strong nonequilibrium effects that cannot be captured by a noninteracting Landauer theory.¹² In the previous work,¹¹ we showed, based on time-dependent density functional theory (TDDFT), that the CT transition can also be induced by an electromagnetic (EM) field (EMF) of photon energy $h\nu = I - A - ezE_z$, without having to increase E_z beyond E_z^* .

The purpose of the present Letter is to study theoretically the effect of such optical transitions on the steady-state current through the molecular junction. Understanding such effects requires a nonequilibrium interacting electron theory as recently developed by two of us.^{2,13–18}

The tunnel junction is modeled by a double quantum dot (QD) Hubbard model, where the first QD (QD₁) represents the state ψ_L localized on the acceptor and the second (QD₂) represents ψ_H of the conjugated donor (see Figure 2). The corresponding Hamiltonian, in Fock space, is given by

Received: August 6, 2014

Accepted: September 19, 2014

Published: September 19, 2014

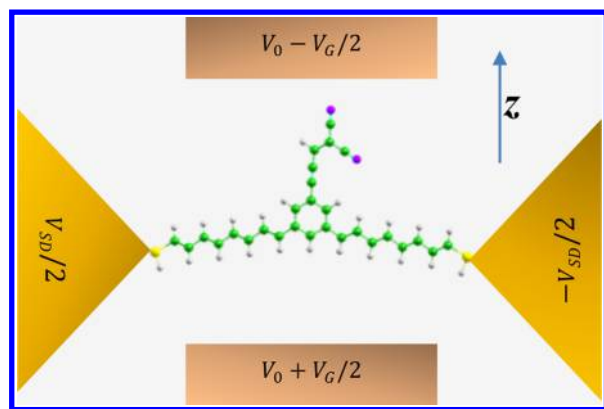


Figure 1. Schematic depiction of the molecular junction. A benzene–malononitrile (MN) acceptor displaced by a vertical distance z with respect to the *trans*-polyacetylene (PA) donor. A gate field is applied parallel to z , thus inducing a gate-dependent potential difference between the donor and acceptor sites. Under these conditions, the energy gap E_g for intramolecular electron transfer becomes dependent on the gate field E_z , $E_g(E_z) = I - A - e z E_z$, where e is the electron charge and I and A are the ionization and affinity energies, respectively. The gate potential V_0 , the gate bias V_G , and the source drain bias V_{SD} are adjustable. DFT calculations showed that a gate field beyond a critical value of $E_z^* = 0.63$ V/Å inspires spontaneous electron transfer from donor (PA) to acceptor (MN). (Reproduced from ref 12 with permission).

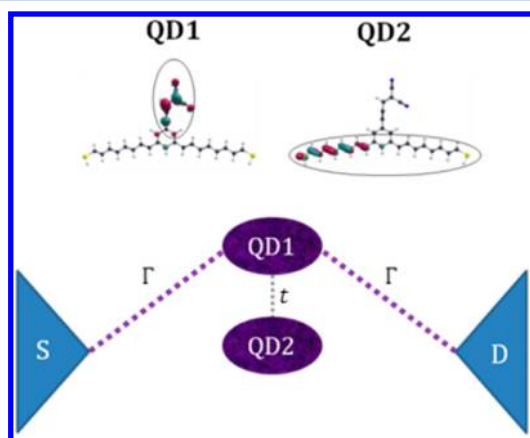


Figure 2. A schematic diagram of the double quantum dot model. QD₁ represents the state ψ_L (localized on the MN acceptor) and QD₂ the state ψ_H (localized on the PA donor) of the molecule. The two QDs couple to each other (with coupling parameter t), but only QD₁ is directly coupled to the SD (with coupling parameter Γ) because of a destructive interference effect.

$$\hat{H}_M^{\text{hub}} = \sum_{i=1}^2 \varepsilon_i(E_z) \hat{n}_i + t \sum_{\sigma=\uparrow\downarrow} (\hat{a}_{1\sigma}^\dagger \hat{a}_{2\sigma} + \text{H.C.}) + \sum_{i=1}^2 U_i \hat{n}_{i\uparrow} \hat{n}_{i\downarrow} + U_{12} (q_1 - \hat{n}_1)(q_2 - \hat{n}_2) - \mu \hat{N} \quad (1)$$

where $\hat{a}_{i\sigma}^\dagger$ ($\hat{a}_{i\sigma}$) are the electron creation (annihilation) operators for QD_{*i*}, and $\hat{n}_{i\sigma} = \hat{a}_{i\sigma}^\dagger \hat{a}_{i\sigma}$ are the spin-dependent occupations ($i = 1, 2$ and $\sigma = \uparrow, \downarrow$); finally, $\hat{n}_i = \hat{n}_{i\uparrow} + \hat{n}_{i\downarrow}$ is the number of electrons, and q_i are the positive charges on each QD. The first term in \hat{H}_M^{hub} describes the single particle site energies, where ε_i is the gate-field-dependent orbital energy of an electron in QD_{*i*}

$$\varepsilon_i(E_z) = \varepsilon_i^0 - e z_i E_z \quad (2)$$

E_z is the gate field in the z direction, and z_i is the vertical position of QD_{*i*} (i.e., $z_1 - z_2 = z$). ε_1^0 is taken as the LUMO energy of the molecule, and ε_2^0 is the HOMO energy of the molecular cation on QD₂. The chemical potential of the leads is μ , and $\hat{N} = \sum_{i=1}^2 \hat{n}_i$ is the number of electrons on the molecule. Under zero bias and gate, the donor site QD₂ is electrically neutral, and because it represents the molecular HOMO, it holds two active electrons and thus also has a static (“nuclear”) charge of $q_2 = 2$. The acceptor site QD₁ is also electrically neutral at zero bias, and because it represents the molecular LUMO, it holds no active electrons and thus has a static charge of $q_1 = 0$. See ref 12 for more details.

The energies of the five low-lying states of the system as a function of the gate field E_z are displayed in Figure 3 within the diabatic limit ($t \rightarrow 0$), where state occupations n_1 and n_2 are good quantum numbers. The actual value of t is small; therefore, the eigenstates of \hat{H}_M^{hub} are similar in character to these diabatic states and can be usefully labeled by the double index (n_1, n_2) . At low gate fields, the ground-state is (02), but as E_z grows, the CT state (11) descends in energy (due to the

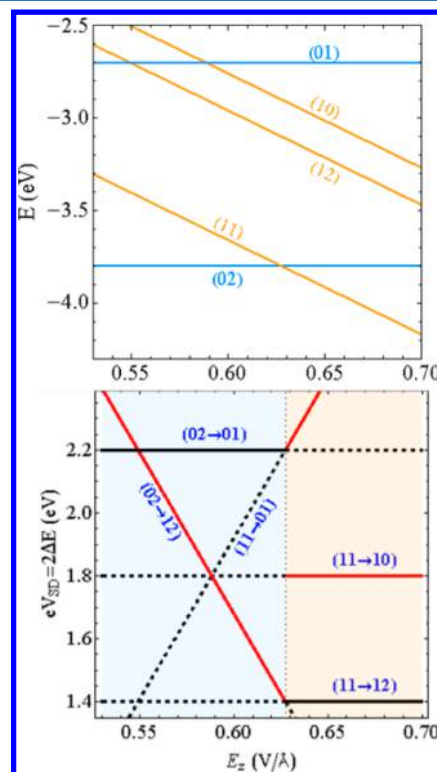


Figure 3. (Top) Low-lying “diabatic” eigenenergies of the junction model as a function of gate field E_z . The states are designated as (n_1, n_2) , where n_i is the occupation of QD_{*i*}. (Bottom) Selected diabatic energy differences (multiplied by 2) from the GS to the nearest hole/electron states as a function of E_z . These can be considered as transition channels in the $V_{SD} - E_z$ plane. The blue (pink) shaded area designates $E_z < E_z^*$ ($E_z > E_z^*$), where (02) ((11)) is the GS. The red lines are the transition channels that should be active under assumption of equilibrium population distribution. The black dotted portion of each line is the regime where this transition channel should not be active due to lack of population of the relevant state. The solid black lines are transition channels that should not be active in the diabatic limit ($t \rightarrow 0$) because in this limit, QD₂ is decoupled from the leads (reproduced from ref 12 with permission).

Table 1. Energetic Parameters of the Many-Body Model, Equations 1, 2, 4, and 5

| parameter | value (eV) | explanation |
|--------------------------------------|------------|---|
| μ | -5.1 | Fermi level of gold |
| ϵ^{HOMO} | -6.2 | from DFT calculation (ref 11) |
| ϵ^{LUMO} | -1.2 | from DFT calculation (ref 11) |
| ϵ_2^0 | -7.8 | ϵ^{HOMO} of PA ⁺ from DFT calculation, (ref 11) |
| ϵ_1^0 | -1.2 | ϵ^{LUMO} from DFT calculation (ref 11) |
| U_1 | 4.5 | α - β splitting after CT, from ref 11 |
| U_2 | 1.6 | $\epsilon^{\text{HOMO}} - \epsilon_1^0$ |
| U_{12} | 1.8 | exciton binding energy from DFT calculation (ref 11) |
| $\Gamma = V_{S_1S_2L} = V_{S_1S_2R}$ | 0.0005 | coupling between molecule and contacts |
| t_{12} | 0.001 | coupling between QD ₁ and QD ₂ |
| $k_B T$ | 0.001 | |
| δ | 0.01 | laser bandwidth |
| $V^{(\text{EM})}$ | 0.001 | optical bath coupling (for transitions (02) \leftrightarrow (11) and (01) \leftrightarrow (10)) |
| parameter | value | explanation |
| N_0 | 1 | laser amplitude (unitless) |
| q_1 | 0 | see text for details |
| q_2 | 2 | see text for details |
| z_1 | 5.1 Å | from ref12 |
| z_2 | 0 | from ref12 |

dependence of ϵ_1 on E_z ; see eq 2). Once $E_z > E_z^*$, where $E_z^* = 0.63 \text{ V/\AA}$, state (11) crosses (02) to become the GS of the system. Three other low-lying states are plotted in Figure 3, the two positively charged states, (01) and (10) and a negatively charged state (12). The energy of states (10) and (12), with $n_1 \neq 0$, is descending with E_z , while the energy of state (01) having $n_1 = 0$ is independent of the gate field. Under the assumption of equilibrium population in the junction, the conductance channels are formed by a transition to low-lying states that differ from the GS by an electron or by a hole. The SD potential difference V_{SD} required for causing a transition $(n_1 n_2) \rightarrow (n_3 n_4)$ is (assuming a symmetric potential drop across the junction)

$$V_{\text{SD}} = \frac{2\Delta E(n_1 n_2 \rightarrow n_3 n_4)}{e} \quad (3)$$

In Figure 3 (bottom), we plot the lines (called “transition channels”) obeying this relation as a function of the gate field E_z .

The full Hamiltonian of the junction with the molecular part written in the many-body states representation is

$$\hat{H} = \hat{H}_M + \hat{H}_K + \hat{H}_{\text{rad}} + \hat{V}_{\text{MK}} + \hat{V}_{\text{EM}} \quad (4)$$

Here, $\hat{H}_M = \sum_{S_1, S_2 \in M} \hat{H}_{S_1 S_2}^{(M)} \hat{X}_{S_1 S_2}$ is the representation of the molecular Hamiltonian \hat{H}_M^{hub} , written in terms of projection operators $\hat{X}_{S_1 S_2} = |S_1\rangle\langle S_2|$ for the molecular many-body states S_1 and S_2 . In the following, we choose diabatic states $(n_1 n_2)$ described above as the many-body basis. The relation between the molecular Hamiltonians \hat{H}_M^{hub} of eq 1 and \hat{H}_M is discussed in more detail in ref 19. $\hat{H}_K = \sum_{k \in L, R} \epsilon_k \hat{c}_k^\dagger \hat{c}_k$ represents the contacts, where \hat{c}_k^\dagger (\hat{c}_k) create (annihilate) an electron in the single-particle state k of the contacts, and $\hat{H}_{\text{rad}} = \sum_{\alpha} \omega_{\alpha} \hat{b}_{\alpha}^\dagger \hat{b}_{\alpha}$ represents the EMF where \hat{b}_{α}^\dagger (\hat{b}_{α}) create (annihilate) a photon in mode α of the field. $\hat{V}_{\text{MK}} = \sum_{S_1, S_2 \in M} \sum_{k \in L, R} (V_{S_1 S_2 k} \hat{X}_{S_1 S_2}^\dagger \hat{c}_k + \text{H.C.})$ describes electron transfer between the molecule and contacts, and $\hat{V}_{\text{EM}} = \sum_{S_1, S_2 \in M} \sum_{\alpha} (V_{S_1 S_2 \alpha}^{(\text{EM})} \hat{X}_{S_1 S_2}^\dagger \hat{b}_{\alpha} + \text{H.C.})$ introduces optical excitations in the molecule due to coupling

to the EMF. Thermal (Fermi–Dirac) population is assumed in the contacts, while laser radiation at frequency ω_0 is modeled as

$$N_{\omega_0}(\omega) = \frac{N_0}{\pi} \frac{\delta^2}{(\omega - \omega_0)^2 + \delta^2} \quad (5)$$

where N_0 characterizes the laser intensity, ω is the EMF frequency, and δ represents the laser bandwidth.

We note that because we are considering a Coulomb blockade, that is, a weak system–bath coupling regime due to intramolecular CT, a simple Redfield quantum master equation (QME) is enough for adequate representation of the model. Below, we use the Redfield QME to simulate populations and current through the junction formed by a molecule coupled to two Fermion baths (representing contacts L and R each at its own equilibrium) and a boson bath (representing the radiation field). The simulation proceeds the usual way; we build the Liouvillian (the Redfieldian), $L = L_M + \sum_{k \in L, R} L_k + L_{\text{rad}}$ and diagonalize it, so that the right eigenvector of the zero eigenvalue of the matrix yields the nonequilibrium density matrix σ . Current at interface K ($=L, R$) is given by $I_K = (e/\hbar) \text{Tr}[\hat{N} L_K \sigma]$, where \hat{N} is the molecular number operator, e is electron charge, and the trace is over the molecular subspace of the problem.²⁰ For the energetic parameters of the model, see Table 1.

We first discuss the effects of spontaneous emission on the tunnel junction; this occurs even in the absence of an external EMF, and after that, we discuss the effects of absorption combined with spontaneous and stimulated emission.

Effects of Spontaneous Emissions. Even in the absence of an externally applied EMF ($N_0 = 0$), the EM coupling $V_{(n_3 n_4)(n_1 n_2) \alpha}^{(\text{EM})}$ introduces an energy dissipation channel for the QP current, in the form of spontaneous photon emission following the transition $(n_3 n_4) \xrightarrow{V^{(\text{EM})}} (n_1 n_2)$. We note that photon emission must preserve the charge state so that $V_{(n_3 n_4)(n_1 n_2) \alpha}^{(\text{EM})}$ can be nonzero only when $n_1 + n_2 = n_3 + n_4$. The dominant effects in our system concern the EM coupling between the neutral states (02) and (11), where for low gate fields (11) $\xrightarrow{V^{(\text{EM})}}$ (02) and for

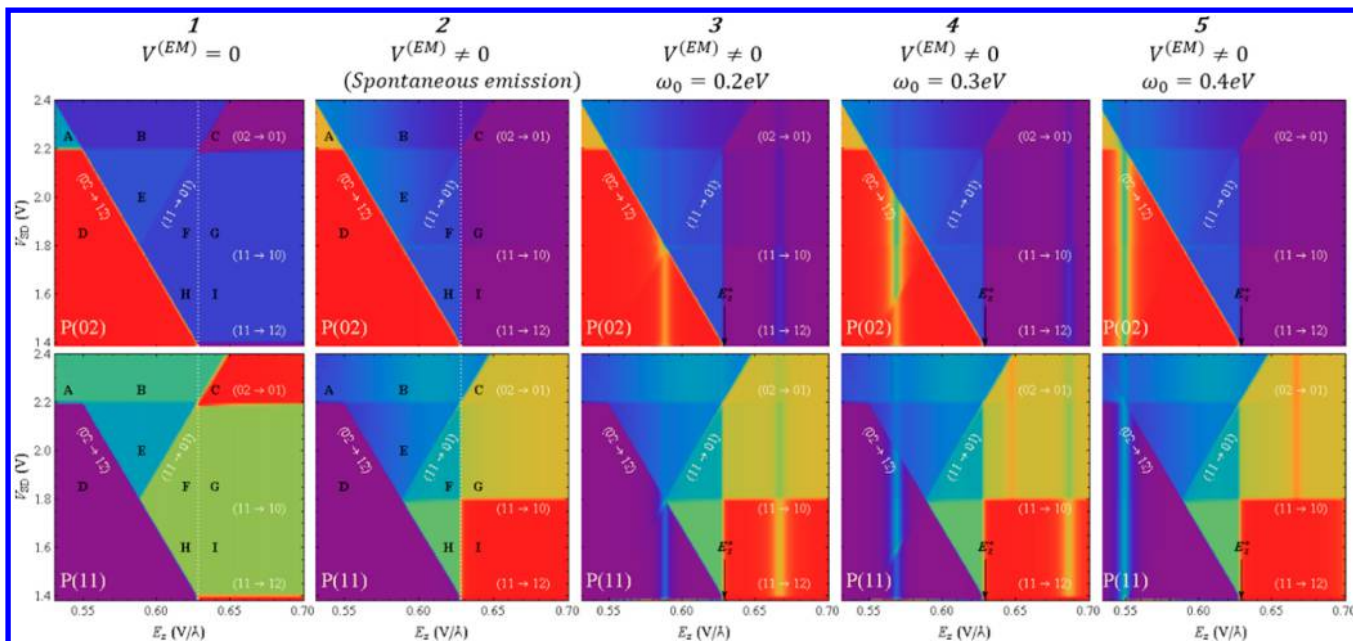


Figure 4. Steady-state population of the states (02) (top panels) and (11) (bottom panels) as a function of the gate and SD potential. Panel 1 correspond to zero EM coupling ($V^{(EM)} = 0$) (which was considered in ref 12), while panels 2–5 correspond to nonzero EM coupling ($V^{(EM)} \neq 0$), for which a spontaneous emission is allowed. Panel 2 displays these populations at zero EMF ($V^{(EM)} = 0, N_0 = 0$), while panels 3–5 are for an EMF with a single photon ($V^{(EM)} \neq 0, N_0 = 1$) for three values of the optical frequencies ω_0 in the infrared domain. Color coding: red = 1; orange = 0.8; yellow = 0.6; green = 0.4; blue = 0.2; and purple = 0.

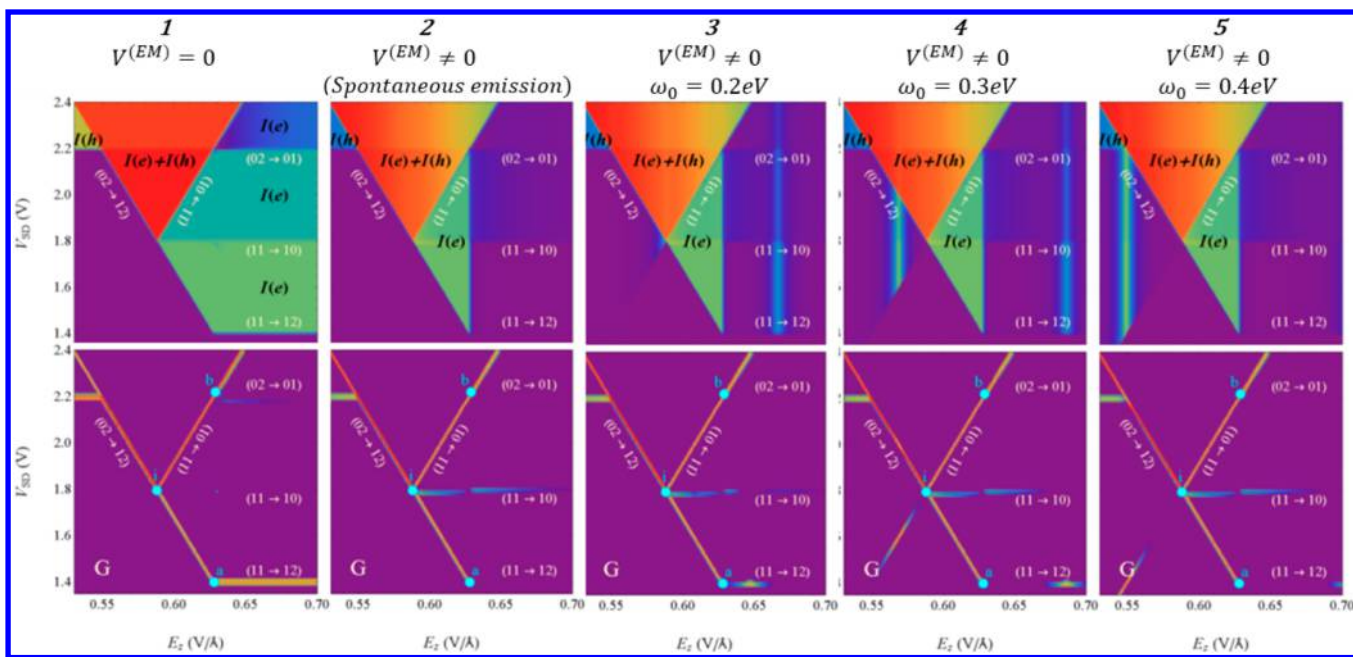


Figure 5. Steady-state current (top panels) and the conductance (bottom panels) for zero EM coupling ($V^{(EM)} = 0$), zero EMF ($V^{(EM)} \neq 0, N_0 = 0$) (panel 2), and for EMF with a single photon ($N_{ph} = 1$) for three values of the optical frequencies ω_0 in the infrared domain (panels 3–5). The color coding for the current and differential conductance peaks has a meaning of intensity (red, orange, yellow, green, blue, and purple, where red is the highest and purple is zero); the maximum current (in atomic units) is $I \approx 1 \times 10^{-5}$, and the maximum conductance is $G \approx 5 \times 10^{-4}$.

high fields $(02) \xrightarrow{V^{(EM)}} (11)$. We denote these two possibilities collectively as $(02) \xleftrightarrow{V^{(EM)}} (11)$. Similar considerations apply to the positively charged states and the transitions $(01) \xleftrightarrow{V^{(EM)}} (10)$. Panels 1 and 2 of Figure 4 compares the population of states (02) and (11) as a function of E_z and V_{SD} for the two cases, where EM coupling is neglected ($V^{(EM)} = 0$)

and where it is allowed (panel 2). In the first case, the coupling between states (02) and (11) is solely due to $H_{(02),(11)}^{(M)}$, a case studied in ref 12. In this case, the steady-state population distribution is nearly constant within regions defined by the red transition lines of Figure 3 (bottom) and changes abruptly when going from one region to the other. This type of discrete behavior was explained in ref 12. In the second case, when EM coupling is allowed, different regions appear due to a new

borderline $E_z = E_z^*$, where E_z^* is the critical gate field. The effect is most striking for the high gate field regime $E_z > E_z^*$, as can be seen in the figure where the EM coupling seems to build a large population of the (11) state at the expense of that of the (02) state (zones G and I in Figure 4, panel 2).

The steady-state population distribution in the junction is closely tied with the steady-state current. Whenever a population of states (02) exists at bias $V_{SD} > 2\Delta E(20-12)/e$, an electron current $I(e)$ is detected, while when a population of state (11) exists at bias $V_{SD} > 2\Delta E(11-01)/e$, a holes current $I(h)$ is noticed. The total current is a combination of the electron and hole currents and is displayed in the top panels of Figure 5. When the EM coupling is turned off (panel 1), the current displays several domains defined by the transition channels of the junction:

(a) a zero current domain, colored purple, obtained at low gate fields, bounded by the two transition channels (02 \rightarrow 12) and (02 \rightarrow 01)

(b) electron and hole currents obtained at the red triangle bounded by the two transition channels (02 \rightarrow 12) and (11 \rightarrow 01)

(c) an electron current domain at high gate fields, bounded by the transition channels (11 \rightarrow 01), (02 \rightarrow 12), and (11 \rightarrow 12)

(d) a hole conducting domain at low gate fields, bounded by the two transition channels (02 \rightarrow 01) and (02 \rightarrow 12)

When the EM coupling is turned on (Figure 5, panel 2), the effect of spontaneous emission is clearly evident at high gate fields ($E_z > E_z^*$), where the current vanishes due to the depletion of (02) population, as discussed above. At low gate fields, the depletion of state (11) reduces the hole current intensity at high bias (the triangle at the upper-left corner, turning from yellow (panel 1) to blue (panel 2)).

Light-Induced Processes in the Junction. The role of the EM coupling is not limited to the relaxation channel emitting a photon, and when light, that is, an external EMF, is introduced, photon absorption and stimulated emission are additional processes that can drive the system. To see these new effects, consider panels 3–5 of Figure 4, which display the (02) (top panel) and (11) (bottom panel) steady-state population in the case when an EMF is present for three values of optical infrared frequencies. It is noticed that sharp ω_0 -dependent features appear on an otherwise similar background. The features appear as (1) sharp depletion in the population of (02) and increase in the population of (11) at a certain $E_z < E_z^*$ and (2) sharp depletion in the population of (11) and increase in the population of (02) at a certain $E_z > E_z^*$. These sharp features occur when $\Delta E(11 \rightarrow 02)$ comes into resonance with the photon energy. Thus, the gate fields E_z for which $\omega_0 = \pm\Delta E(11 \rightarrow 02)$ are those at which the effects are seen (note that when $E_z = E_z^*$, we have $\Delta E(11 \rightarrow 02) = 0$). Increasing ω_0 shifts the vertical lines away from E_z^* in a symmetric way. An additional feature in Figure 4 is relevant for the (11) populations but not for those of (02). These lines (at $E_z \approx 0.65$ V/Å, for $\omega_0 = 0.3$ eV, and at $E_z \approx 0.68$ V/Å, for $\omega_0 = 0.4$ eV) are caused by the transition of populations from the (10) to the (01) states, a change that has an effect on the (11) population because of the hole conducting channel (11 \rightarrow 01) described in the caption of Figure 3.

As seen in Figure 4, upon an excitation, a population of state (11) ((02)) is accumulated at low (high) gate fields $E_z < E_z^*$ ($E_z > E_z^*$), while a population of state (02) ((11)) is depleted. These will affect the current as these populations can conduct

holes or electrons. Current will transport through the junction if the SD bias is higher than the relevant transition channels, that is, $V_{SD} > 2\Delta E(11 \rightarrow 01)$ or $V_{SD} > 2\Delta E(02 \rightarrow 12)$. At $\omega_0 = 0.3$ eV, two EMF-induced current features appear as bluish lines at the current map (top panel of Figure 5), one at low gate field $E_z \approx 0.57$ V/Å and one at high gate field $E_z \approx 0.69$ V/Å. At low

gate field, the EMF stimulates an absorption (02) $\xrightarrow{V^{(EM)}} (11)$; thus, a population of state (11) is now present at this low gate field, and for a SD bias higher than $2\Delta E(11 \rightarrow 01)$, it conducts holes. At high gate field, the EMF stimulates an absorption

(11) $\xrightarrow{V^{(EM)}} (02)$; thus, a population of state (02) is now present at high gate field, and for a SD bias higher than $2\Delta E(02 \rightarrow 12)$, it conducts electrons. When the EMF is tuned to a higher frequency $\omega_0 = 0.4$ eV, only the hole-induced current regime is displayed at $E_z \approx 0.59$ V/Å. The electron current induced by the EMF is obtained at higher gate field ($E_z \approx 0.71$ V/Å) and thus cannot be seen here. However, when the frequency of the EMF is tuned to $\omega_0 = 0.2$ eV, although both absorption transitions occur, that is, (02) $\xrightarrow{V^{(EM)}} (11)$ and (11) $\xrightarrow{V^{(EM)}} (02)$ (see panel 3, top and bottom of Figure 4), only the latter induces current in the junction (an electron current). At this

ω_0 , the transition (02) $\xrightarrow{V^{(EM)}} (11)$ occurs at gate field $E_z = 0.59$ V/Å, for which the criteria $V_{SD} > 2\Delta E(11 \rightarrow 01)$ is met only at high biases where a steady-state population of state (11) is already dominant; thus, the effect induced by the EMF can hardly be seen. The appearance of EMF-induced current regimes creates modulations on the conductance channels. The most dominant effect here can be seen for $\omega_0 = 0.3$ and 0.4 eV, where the (11 \rightarrow 01) conducting channel continues to low gate field.

To summarize, we have studied the effect of an EM coupling on the steady-state population current and conductance of the junction depicted in Figure 1 under an external gate field and SD bias. This junction was considered in our previous paper where it was described by a double quantum dot Hubbard Hamiltonian and analyzed within a nonequilibrium many-body approach based on the Redfield theory.¹² We show that even in the absence of an EMF, the addition of the EM coupling has a large effect on the steady-state population and current because it introduces a relaxation channel via a process of spontaneous emission. The effect of spontaneous emission is more pronounced at high gate fields ($E_z > E_z^*$), where the excited-state (02) population is depleted while building up the GS population of state (11). Within this framework, the role of E_z^* as a borderline between the ground and excited state populations becomes more decisive, revealing the sharp switching response of the junction to the threshold gate field value. The sharp switching behavior can be seen in the top panels of Figure 5, where the electron current $I(e)$ vanishes once $E_z > E_z^*$. Note that this is not the case when EM coupling is absent, as can be seen in panel 1 (top) of Figure 5.

Upon turning on an EMF with an optical frequency ω_0 , the population distribution is preserved but displays two additional sharp lines. These lines appear at gate fields where the energy of the EMF photon induces a resonance between the two neutral electronic states, namely, $\hbar\omega_0 = \Delta E(11 \leftrightarrow 02)$, where ΔE is a function of E_z (see the top panel of Figure 3). Because at $E_z = E_z^*$, $\Delta E(11 \leftrightarrow 02) = 0$, the lines appear in a symmetric pattern with regard to E_z^* . The changes of population induce changes in the current. Thus, for low gate fields ($E_z < E_z^*$), a depletion of

state (02) follow by a buildup of state (11) induces a current of holes via the conducting channel (11 \rightarrow 01). At high gate fields ($E_z > E_z^*$), a depletion of state (11) followed by a buildup of state (02) induces an electron current via the conducting channel (02 \rightarrow 12). Thus, the DC gate field and the AC EMF enable separately and in various combinations a sharp switching of several aspects of the electronic behavior of the molecular junction.

AUTHOR INFORMATION

Notes

The authors declare no competing financial interest.

ACKNOWLEDGMENTS

R.B. gratefully thanks the U.S.–Israel Binational Science Foundation (BSF) for support of this work. M.G. gratefully thanks the Department of Energy (Early Career Award, DE-SC0006422) for support of this research. A.W. acknowledges support of the U.S. Department of Energy through the Los Alamos National Laboratory (LANL) Center for Nonlinear Studies (CNLS). LANL is operated by Los Alamos National Security, LLC, for the National Nuclear Security Administration of the U.S. Department of Energy under Contract DE-AC52-06NA25396.

REFERENCES

- (1) Vadai, M.; Nachman, N.; Ben-Zion, M.; Burkle, M.; Pauly, F.; Cuevas, J. C.; Selzer, Y. Plasmon-Induced Conductance Enhancement in Single-Molecule Junctions. *J. Phys. Chem. Lett.* **2013**, *4*, 2811–2816.
- (2) Galperin, M.; Nitzan, A. Molecular Optoelectronics: The Interaction of Molecular Conduction Junctions with Light. *Phys. Chem. Chem. Phys.* **2012**, *14*, 9421–9438.
- (3) Sukharev, M.; Galperin, M. Transport and Optical Response of Molecular Junctions Driven by Surface Plasmon Polaritons. *Phys. Rev. B* **2010**, *81*, 165307.
- (4) Odell, A.; Delin, A.; Johansson, B.; Rungger, I.; Sanvito, S. Investigation of the Conducting Properties of a Photoswitching Dithienylethene Molecule. *ACS Nano* **2010**, *4*, 2635–2642.
- (5) Smaali, K.; Lenfant, S.; Karpe, S.; Ocafrain, M.; Blanchard, P.; Deresmes, D.; Godey, S.; Rochefort, A.; Roncali, J.; Vuillaume, D. High On–Off Conductance Switching Ratio in Optically-Driven Self-Assembled Conjugated Molecular Systems. *ACS Nano* **2010**, *4*, 2411–2421.
- (6) van der Molen, S. J.; Liljeroth, P. Charge Transport through Molecular Switches. *J. Phys.: Condens. Matter* **2010**, *22*, 133001.
- (7) Russew, M.-M.; Hecht, S. Photoswitches: From Molecules to Materials. *Adv. Mater.* **2010**, *22*, 3348–3360.
- (8) Irie, M. Diarylethenes for Memories and Switches. *Chem. Rev.* **2000**, *100*, 1685–1716.
- (9) Wang, L.; May, V. Optical Switching of Charge Transmission through a Single Molecule: Effects of Contact Excitations and Molecule Heating. *J. Phys. Chem. C* **2010**, *114*, 4179–4185.
- (10) Zelinsky, Y.; May, V. Photoinduced Switching of the Current through a Single Molecule: Effects of Surface Plasmon Excitations of the Leads. *Nano Lett.* **2011**, *12*, 446–452.
- (11) Baratz, A.; Baer, R. Nonmechanical Conductance Switching in a Molecular Tunnel Junction. *J. Phys. Chem. Lett.* **2012**, *3*, 498–502.
- (12) Baratz, A.; Galperin, M.; Baer, R. Gate-Induced Intramolecular Charge Transfer in a Tunnel Junction: A Nonequilibrium Analysis. *J. Phys. Chem. C* **2013**, *117*, 10257–10263.
- (13) White, A. J.; Tretiak, S.; Galperin, M. Raman Scattering in Molecular Junctions: A Pseudoparticle Formulation. *Nano Lett.* **2014**, *14*, 699–703.
- (14) White, A. J.; Fainberg, B. D.; Galperin, M. Collective Plasmon–Molecule Excitations in Nanojunctions: Quantum Consideration. *J. Phys. Chem. Lett.* **2012**, *3*, 2738–2743.

(15) White, A. J.; Ochoa, M. A.; Galperin, M. Nonequilibrium Atomic Limit for Transport and Optical Response of Molecular Junctions. *J. Phys. Chem. C* **2014**, *118*, 11159–11173.

(16) Oren, M.; Galperin, M.; Nitzan, A. Raman Scattering from Molecular Conduction Junctions: Charge Transfer Mechanism. *Phys. Rev. B* **2012**, *85*, 115435.

(17) Galperin, M.; Tretiak, S. Linear Optical Response of Current-Carrying Molecular Junction: A Nonequilibrium Green's Function-Time-Dependent Density Functional Theory Approach. *J. Chem. Phys.* **2008**, *128*, 124705.

(18) Selzer, Y.; Peskin, U. Transient Dynamics in Molecular Junctions: Picosecond Resolution from dc Measurements by a Laser Pulse Pair Sequence Excitation. *J. Phys. Chem. C* **2013**, *117*, 22369–22376.

(19) Esposito, M.; Galperin, M. Transport in Molecular States Language: Generalized Quantum Master Equation Approach. *Phys. Rev. B* **2009**, *79*, 205303.

(20) Breuer, H.-P.; Petruccione, F. *The Theory of Open Quantum Systems*; Oxford University Press: Oxford, U.K.; New York, 2002.